

# Submillimetre observations of WISE-selected high-redshift, luminous, dusty galaxies

Suzy F. Jones,<sup>1\*</sup> Andrew W. Blain,<sup>1</sup> Daniel Stern,<sup>2</sup> Roberto J. Assef,<sup>3</sup> Carrie R. Bridge,<sup>4</sup> Peter Eisenhardt,<sup>2</sup> Sara Petty,<sup>5</sup> Jingwen Wu,<sup>6</sup> Chao-Wei Tsai,<sup>2</sup> Roc Cutri,<sup>7</sup> Edward L. Wright<sup>6</sup> and Lin Yan<sup>7</sup>

<sup>1</sup> *University of Leicester, X-ray and Observational Astronomy Group (XROA), Department of Physics & Astronomy, University Road, Leicester LE1 7RH, UK*

<sup>2</sup> *Jet Propulsion Laboratory, California Institute of Technology, 4800 Oak Grove Dr., Pasadena, CA 91109, USA*

<sup>3</sup> *Núcleo de Astronomía de la Facultad de Ingeniería, Universidad Diego Portales, Av. Ejército Libertador 441, Santiago, Chile*

<sup>4</sup> *California Institute of Technology MS249-17, Pasadena, CA, 91125, USA*

<sup>5</sup> *Virginia Polytechnic Institute & State University, Department of Physics MC 0435, 850 West Campus Drive, Blacksburg, VA 24061, USA*

<sup>6</sup> *Division of Physics & Astronomy, University of California Los Angeles, Physics and Astronomy Building, 430 Portola Plaza, Los Angeles, CA 90095-1547, USA*

<sup>7</sup> *Infrared Processing and Analysis Center, California Institute of Technology, MS 100-22, Pasadena, CA 91125, USA*

Submitted xx/xx/2014

## ABSTRACT

We present SCUBA-2 850  $\mu\text{m}$  submillimetre (submm) observations of the fields of 10 dusty, luminous galaxies at  $z \sim 1.7 - 4.6$ , detected at 12  $\mu\text{m}$  and/or 22  $\mu\text{m}$  by the WISE all-sky survey, but faint or undetected at 3.4  $\mu\text{m}$  and 4.6  $\mu\text{m}$ ; dubbed hot, dust-obscured galaxies (Hot DOGs). The six detected targets all have total infrared luminosities greater than  $10^{13} L_{\odot}$ , with one greater than  $10^{14} L_{\odot}$ . Their spectral energy distributions (SEDs) are very blue from mid-infrared to submm wavelengths and not well fitted by standard AGN SED templates, without adding extra dust extinction to fit the WISE 3.4  $\mu\text{m}$  and 4.6  $\mu\text{m}$  data. The SCUBA-2 850  $\mu\text{m}$  observations confirm that the Hot DOGs have less cold and/or more warm dust emission than standard AGN templates, and limit an underlying extended spiral or ULIRG-type galaxy to contribute less than about 2% or 55% of the typical total Hot DOG IR luminosity, respectively. The two most distant and luminous targets have similar observed submm to mid-infrared ratios to the rest, and thus appear to have even hotter SEDs. The number of serendipitous submm galaxies (SMGs) detected in the 1.5-arcmin-radius SCUBA-2 850  $\mu\text{m}$  maps indicates there is a significant over-density of serendipitous sources around Hot DOGs. These submm observations confirm that the WISE-selected ultra-luminous galaxies have very blue mid-infrared to submm SEDs, suggesting that they contain very powerful AGN, and are apparently located in unusual arcmin-scale overdensities of very luminous dusty galaxies.

**Key words:** galaxies: active – galaxies: high-redshift – galaxies: formation – infrared: galaxies – submillimetre: galaxies

## 1 INTRODUCTION

Ultra-Luminous Infrared Galaxies (ULIRGs)<sup>1</sup> were first discovered in the 1980's by the *Infrared Astronomical Satellite*

\* E-mail: sfj8@le.ac.uk

<sup>1</sup> LIRGs, ULIRGs and HyLIRGs have characterising total infrared luminosities (8-1000  $\mu\text{m}$ ) of  $L_{8-1000\mu\text{m}} > 10^{11} L_{\odot}$ ,  $L_{8-1000\mu\text{m}} > 10^{12} L_{\odot}$  and  $L_{8-1000\mu\text{m}} > 10^{13} L_{\odot}$

(*IRAS*) (Houck et al. 1984; Soifer et al. 1984). More than 90% of their luminosity is emitted in the infrared (IR) due to interstellar dust absorbing ultraviolet (UV) and optical emission produced by active galactic nuclei (AGN) and/or starbursts. The dust then re-emits thermally at longer wavelengths, from the near-IR to millimetre (mm) wavebands.

ULIRGs evolve strongly with redshift, becoming more abundant with a surface density of several hundred per square degree at  $z \sim 1$ . Out to  $z \sim 1$  the evolution rate of luminous dusty galaxies goes as  $\sim (1+z)^4$  (Blain et al. 1999; Le Floc'h et al. 2005a). To  $z \geq 1$  ULIRGs along with Luminous Infrared Galaxies (LIRGs),<sup>1</sup> account for  $70 \pm 15\%$  of cosmic star formation activity (Le Floc'h et al. 2005b; Richards et al. 2006). Therefore, at the peak of the cosmic star formation rate,  $z \sim 2-3$ , ULIRGs contribute a significant amount to the total IR luminosity density (Smail et al. 1997; Genzel & Cesarsky 2000; Blain et al. 2002; Cowie et al. 2002; Chapman et al. 2005; Le Floc'h et al. 2005b; Hopkins et al. 2008; Reddy et al. 2008; Magnelli et al. 2009; Elbaz et al. 2011; Casey et al. 2012; Magnelli et al. 2012; Melbourne et al. 2012; Lu et al. 2013). Studying the most extreme IR galaxies at this epoch, should provide a larger and more complete sample of different types of the most luminous AGN, to help in fully understanding the processes of formation and evolution of massive galaxies.

A popular theory for the origin of ULIRGs is that major mergers between massive, gas-rich galaxies provide tidal torques that transport gas to the centre of the more massive galaxy (Barnes & Hernquist 1992; Schweizer 1998; Farrah et al. 2001; Veilleux et al. 2002; Hopkins et al. 2006, 2008). This influx of gas can induce rapid star formation and/or AGN fuelling (Barnes & Hernquist 1992; Mihos 1996; Hopkins et al. 2008): starburst activity dominates the luminosity at first, and then the embedded supermassive black hole (SMBH) grows to dominate. Feedback from the SMBH (radiation, winds and/or jets) and supernovae can expel gas and dust, terminating further star formation and for a short time leaving a visible optical quasar (QSO): finally, a passive massive elliptical galaxy is left behind (Sanders & Mirabel 1996; Hopkins et al. 2006, 2008; Farrah et al. 2012; Spoon et al. 2013). Observations of other dusty galaxy populations could be evidence of different stages of this merging galaxy theory. For example, submillimetre galaxies (SMGs) appear to be high redshift ULIRGs (Blain et al. 2002; Tacconi et al. 2008) and dust-obscured galaxies (DOGs) have comparable star formation rates and IR luminosities to SMGs (Bussmann et al. 2009; Tyler et al. 2009; Melbourne et al. 2012). There could be an evolutionary connection between ULIRGs, SMGs, DOGs, QSOs and massive elliptical galaxies (Sanders et al. 1988a,b).

Luminous, dusty active galaxies heated by AGN and/or recent starburst activity emit in the IR at wavelengths traced by the *Wide-field Infrared Survey Explorer* (WISE) filters at  $12\mu\text{m}$  (W3) and  $22\mu\text{m}$  (W4) bands. Eisenhardt et al. (2012), Wu et al. (2012) and Bridge et al. (2013, in prep.) have shown that WISE can find different classes of interesting, luminous, high-redshift, dusty galaxies. Based on WISE colours and flux cuts, a population has faint or undetectable flux densities in the  $3.4\mu\text{m}$  (W1) and  $4.6\mu\text{m}$  (W2) bands, while being well detected (signal-to-noise ratio (SNR)  $> 5$  in the All-Sky WISE Source Cata-

$\log^2$ ) in the  $12$  and/or  $22\mu\text{m}$  bands. These galaxies have been called “W1W2-dropouts” (Eisenhardt et al. 2012) and Hot DOGs (Wu et al. 2012).

In the major merger theory, the SMG population would represent an earlier, starburst-dominated phase of merging galaxies, and the luminous DOG population are the later, most luminous AGN-dominated phase of merging galaxies, and in energetic terms could easily become optically visible QSOs (Narayanan et al. 2010). The Hot DOGs presented in this paper would qualify the DOG selection criterion,  $F_{24\mu\text{m}} > 0.3$  mJy and  $R-[24] > 14$  (where  $R$  is the Vega magnitudes for optical  $R$  band and *Spitzer* mid-IR  $24\mu\text{m}$  (Dey et al. 2008)) however, the Hot DOGs are more luminous, hotter and rarer than typical DOGs and could be extreme cases of DOGs or another stage of merging galaxies (Wu et al. 2012). To investigate this Hot DOG population, follow-up spectroscopy of more than 100 of them revealed that these galaxies are intrinsically very luminous, potentially putting them in the class of ULIRGs<sup>1</sup> and Hyper-Luminous Infrared Galaxies (HyLIRGs)<sup>1</sup> (Sanders & Mirabel 1996; Lonsdale et al. 2006) (Bridge et al. 2013, in prep.; Eisenhardt et al. in prep.; Tsai et al. in prep.). They are frequently found in the redshift range  $2 < z < 3$  (Eisenhardt et al. 2012; Wu et al. 2012; Bridge et al. 2013), and so far the highest redshift is  $z = 4.59$  for W2246-0526 (Tsai et al. in prep.). Their SEDs show a mid-IR to far-IR colour that is too blue to be well fitted by many standard AGN templates, suggesting that they represent a short evolutionary phase of merging galaxies, where an AGN is fueling very rapidly inside a thick dust shroud, leading to very intense mid-IR but obscured emission and a hot SED, as proposed by (Wu et al. 2012; Bridge et al. 2013; Assef et al. in prep.). The Hot DOGs should show the impact of an AGN on the surrounding ISM at its very greatest. These WISE-selected sources are certainly not typical galaxies, but the processes taking place within them should be at work everywhere.

In this paper, James Clerk Maxwell Telescope (JCMT) Submillimetre Common-User Bolometer Array 2 (SCUBA-2) (Holland et al. 2013) observations of 10 Hot DOGs are reported. These long wavelength measurements are needed to understand the cold dust properties and to calculate the total luminosity all the way from  $8\mu\text{m}$  to  $1000\mu\text{m}$  ( $L_{8-1000\mu\text{m}}$ ). Section 2 describes the sample, along with the details of WISE and SCUBA-2 observations. Section 3 reports the SCUBA-2 results, and the SEDs and total IR luminosities ( $L_{8-1000\mu\text{m}}$ ) of the Hot DOGs in comparison with other populations. Existing SED templates of well-studied objects are compared to find out the nature of the Hot DOGs, and their accuracy and a need for additional mid-IR extinction to fit the data is discussed. The submm to mid-IR ratios are discussed, to investigate if the Hot DOG SEDs are dominated by AGN emission or star formation. The luminosities of an underlying extended host galaxy component are calculated, in order to calculate the potential host galaxy contribution to the typical Hot DOG total IR luminosity, to see if the Hot DOGs are dominated by AGN or starburst activity. To see if there is an overdensity of SMGs in the

<sup>2</sup> <http://wise2.ipac.caltech.edu/docs/release/allsky/>

SCUBA-2 fields, SMG number counts are compared to those in other submm surveys.

Throughout this paper we assume a  $\Lambda$ CDM cosmology with  $H_0 = 71 \text{ km s}^{-1} \text{ Mpc}^{-1}$ ,  $\Omega_m = 0.27$  and  $\Omega_\Lambda = 0.73$  (Hinshaw et al. 2009). WISE catalogue magnitudes are converted to flux densities using zero-point values on the Vega system of 306.7, 170.7, 29.04 and 8.284 Jy for WISE 3.4, 4.6, 12 and 22  $\mu\text{m}$  wavelengths, respectively (Wright et al. 2010).

## 2 OBSERVATIONS

### 2.1 WISE

WISE was launched in December 2009 and surveyed the entire sky at wavelengths of 3.4, 4.6, 12 and 22  $\mu\text{m}$  (Wright et al. 2010). One of the primary science goals was to identify the most luminous galaxy in the observable universe, which can be accomplished due to WISE obtaining much greater sensitivity than previous all-sky IR survey missions. For example, *IRAS* yielded catalogued source sensitivities of 0.5 Jy at 12, 25 and 60  $\mu\text{m}$  and 1 Jy at 100  $\mu\text{m}$  (Neugebauer et al. 1984). WISE achieved 5- $\sigma$  source sensitivities better than 0.054, 0.071, 0.73 and 5.0 mJy and angular resolutions of 6.1, 6.4, 6.5 and 12.0 arcsec in the W1 to W4 bands, respectively (Wright et al. 2010; Jarrett et al. 2011).

### 2.2 Target Selection

The objects observed here are selected from the WISE All-Sky Source catalog<sup>2</sup>, with IR magnitudes derived using point source profile-fitting (Cutri et al. 2012). The Hot DOG selection criteria are to have a faint or undetectable flux in W1 and W2, but a detectable flux ( $\text{SNR} > 5$ ) in W3 and/or W4. The selected galaxies have  $W1 > 17.4$  mag and either  $W4 < 7.7$  mag and  $W2 - W4 > 8.2$  or  $W3 < 10.6$  mag and  $W2 - W3 > 5.3$  (Eisenhardt et al. 2012). The search was made greater than  $30^\circ$  away from the Galactic centre and  $10^\circ$  from the Galactic plane to avoid enhanced levels of saturation artifacts and stars.

The number of WISE-selected Hot DOGs over the extragalactic sky, to this magnitude limit, is about 1000, which points to this population being extremely rare, and perhaps a transitional population (Eisenhardt et al. 2012; Assef et al. in prep.; Tsai et al. in prep.). The JCMT targets were selected because they had known spectroscopic redshifts (Eisenhardt et al. 2012, in prep.; Bridge et al. in prep.), could be observed in the A-semester (January to July) at the JCMT, and were queued to obtain *Herschel* data (Bridge et al. in prep.; Tsai et al. in prep.). We selected 31 targets and obtained observations of 10 targets with SCUBA-2 that were chosen at random due to the vagaries of the queue observing system. Their WISE W4 band fluxes were selected to be among the greatest of the suitable sources, in the hope of increasing the chance that their 850  $\mu\text{m}$  flux would be bright enough to be detected or limits would be significant. Therefore, with any conclusions drawn it must be remembered that these Hot DOGs have been selected to be mid-IR bright.

The WISE flux densities presented in Table 1 are from

the subsequent AllWISE Source Catalog<sup>3</sup>, that has improved photometric sensitivity and accuracy, and improved astrometric precision compared to the WISE All-Sky Source Catalog.

### 2.3 JCMT SCUBA-2

Ten Hot DOGs were observed with SCUBA-2 on the 15-m JCMT atop Mauna Kea in Hawaii, primarily in May 2012 but also on other nights throughout the 12A semester, from January to July 2012.

SCUBA-2 is a bolometer camera and has eight 32 x 40 pixel detector arrays each with a field of view of 2.4 arcmin<sup>2</sup> (Holland et al. 2013). SCUBA-2 observes in the atmospheric windows at 450  $\mu\text{m}$  and 850  $\mu\text{m}$ . The diffraction-limited beams have full-width half maxima (FWHM) of approximately 7.5 and 14.5 arcsec, respectively.

The optical depth at 225 GHz,  $\tau_{225}$ , during the observations was in the range of JCMT Band 2 conditions:  $0.05 < \tau_{225} < 0.08$  (Dempsey et al. 2013). The corresponding opacities for each atmospheric window, 450  $\mu\text{m}$  and 850  $\mu\text{m}$ , were  $0.61 < \tau_{450} < 1.18$  and  $0.24 < \tau_{850} < 0.40$ . Therefore, we could not use any 450  $\mu\text{m}$  data because the atmospheric opacity was too great.

All observations were taken in the “CV DAISY” mode that produces a 12-arcmin diameter map, with the deepest coverage in a central 3-arcmin diameter region (Holland et al. 2013). The target stays near the centre of the arrays and the telescope performs a pseudo-circular pattern with a radius of 250 arcsec at a speed of 155 arcsec s<sup>-1</sup>. This mode is best for point-like sources and those smaller than 3-arcmin. Each scan was 30 minutes long and four scans were made per target, totalling a exposure time of 120 minutes per target. The typical 850  $\mu\text{m}$  noise achieved in these DAISY maps was 1.8 mJy/beam, and the noise increases by  $\sim 10\%$  out to a radius of 1.5 arcmin (Table 1). We have treated only this uniform central region of the SCUBA2 DAISY maps in this analysis.

Pointing checks were taken throughout the night. The calibration sources observed were Uranus, CRL 2688, CRL 618 and Mars. Calibrations were taken at the start and end of every night in the standard manner (Dempsey et al. 2013), and where consistent with the standard values.

## 3 RESULTS

### 3.1 Photometry

The maps were reduced with the STARLINK SubMillimeter User Reduction Facility (SMURF) data reduction package with the “Blank Field” configuration suitable for low SNR point sources (Chapin et al. 2013). SMURF performs pre-processing steps to clean the data by modelling each of the contributions to the signal from each bolometer, flat-fields and removes atmospheric emission, and finally regrids to produce a science-quality image. Using the STARLINK Pipeline for Combining and Analyzing Reduced Data (PICARD) package the maps were mosaiced with all four observations per target, beam-match filtered with a 15 arcsec

<sup>3</sup> <http://wise2.ipac.caltech.edu/docs/release/allwise/>

FWHM Gaussian and calibrated with the flux conversion factor (FCF) of  $2.34 \text{ Jy pW}^{-1} \text{ arcsec}^{-2}$  (appropriate for aperture photometry) or  $537 \text{ Jy pW}^{-1} \text{ beam}^{-1}$  (in order to measure absolute peak fluxes of discrete sources) that is appropriate for  $850 \mu\text{m}$  data (Dempsey et al. 2013).

The  $850 \mu\text{m}$  flux densities of the 10 Hot DOGs at their WISE positions and the noise level in the maps are presented in Table 1. Six Hot DOGs are detected at greater than  $3\sigma$  significance, while the other four targets had positive flux measurements at the WISE position with significances between  $1.1\sigma$  and  $1.9\sigma$ . The flux density limits for all the targets were measured in an aperture diameter of  $15 \text{ arcsec}$ , which is the same size as the FWHM of the telescope beam. This was an appropriate aperture size: for the detected sources, the aperture flux densities on this scale are consistent with the peak flux densities. Figure 1 and Figure 2 show the sensitive 3-arcmin diameter SCUBA-2  $850 \mu\text{m}$  DAISY fields of the 6 detected Hot DOGs and the 4 undetected Hot DOGs, respectively. The typical error of the WISE position compared to the SCUBA-2 position of the detected targets was  $1 \text{ arcsec}$ .

To test whether the positive flux density of the four targets with upper limits is likely to be real, random points were sampled from the maps, and the stacked average flux density was  $0.0 \pm 0.5 \text{ mJy}$ . This is consistent with the positive flux densities from the Hot DOGs with upper limits being due to fainter, undetected targets.

W2026+0716 is the only target whose  $850 \mu\text{m}$  flux increases when measured in a larger aperture (see Figure 3). It has a  $850 \mu\text{m}$  flux density of  $2.1 \text{ mJy}$  with a  $15\text{-arcsec}$  beam-sized aperture. However, when increasing the diameter to  $29 \text{ arcsec}$ , the flux density increases to  $7.3 \text{ mJy}$ . The higher flux is likely because the target has multiple components on scales bigger than the SCUBA-2 beam. Multiple components have been seen in another Hot DOG, W1814+3412, where several objects on scales less than  $10 \text{ arcsec}$  are apparent (Eisenhardt et al. 2012). Alternatively, there could be an unrelated source or sources. The WISE extended source flag is 0 for the W1 through W4 bands, which means that the detected source is not extended at WISE wavelengths (see Figure 3). There are no obvious signs of a cluster of sources nearby in *Spitzer* images (Wu et al. priv. comm.). However, *Herschel*  $160 \mu\text{m}$  imaging shows a possible companion about  $10 \text{ arcsec}$  away that could contribute enhanced flux in larger apertures in this source (Bridge et al. priv. comm.). Due to this uncertainty, the quoted  $850 \mu\text{m}$  flux density in Table 1 is the  $15\text{-arcsec}$  beam-sized aperture flux density ( $2.1 \text{ mJy}$ ).

When the images of the four undetected sources are stacked together into one image (Figure 4) and centred on the WISE-determined position of each target, the net flux is  $7.8 \pm 2.3 \text{ mJy}$  in the central  $15 \text{ arcsec}$  region, a net detection of  $3.4\sigma$ . The four undetected targets are consistent with being on average 2.5 times fainter than the six detected targets. To get deeper observations with SCUBA-2 would require several more hours of integration per target, beyond the existing 120 minutes, but would not add much more value to this stacked result.

The flux densities presented in Table 1 can be compared with the results of Wu et al. (2012), who observed 14 WISE-selected Hot DOGs with the Caltech Submillimeter Observatory (CSO) SubMillimeter High Angular Resolution Camera II (SHARC-II) at  $350$  to  $850 \mu\text{m}$  and 18 Hot



**Figure 4.** SCUBA-2  $850 \mu\text{m}$   $48 \text{ arcsec}$  radius map showing the central region of the 4 undetected targets stacked together. The cross shows the central pixel. North is up, East is to the left.

DOGs with CSO Bolocam at  $1.1 \text{ mm}$ . Using a  $3\sigma$  threshold, Wu et al. (2012) found that nine out of 14 Hot DOGs were detected at  $350 \mu\text{m}$  and 6 of the 18 targets were detected at  $1.1 \text{ mm}$ . Three sources from the Hot DOG sample in this paper were in common with Wu et al. (2012); W1603+2745, W1814+3412 and W1835+4355. These CSO results are consistent with our SCUBA-2 observations at  $850 \mu\text{m}$ . The relative sensitivities of SHARC-II and Bolocam are such that we believe the SCUBA-2 detections and limits provide a substantial increase in our knowledge of the HotDOGs' submm properties. Furthermore, W1814+3412 which was detected at  $350 \mu\text{m}$  by Wu et al. (2012), with upper limits reported at  $450 \mu\text{m}$  and  $1100 \mu\text{m}$  was also detected by the Institut de Radioastronomie Millimetrique (IRAM) Plateau de Bure interferometer in the  $1.3 \text{ mm}$  band in 2013 (Blain et al. in prep.).

## 3.2 SEDs

### 3.2.1 Short Wavelength SEDs

The SEDs of the 10 SCUBA-2 Hot DOGs are shown in Figure 5. The SEDs are normalised at rest-frame  $3 \mu\text{m}$  and shown at rest-frame wavelengths in order to compare to various galaxy SED templates (Polletta et al. 2007) in order to try and understand the Hot DOGs nature. The Polletta galaxy templates are Arp 220 (starburst-dominated galaxy), Mrk 231 (heavily obscured AGN-starburst composite), QSO 1 and 2 (optically-selected QSOs of Type 1 and 2) and torus (type-2 heavily-obscured QSO: an accreting SMBH with a hot accretion disk surrounded by dust and Compton-thick gas in a toroidal structure (Krolik & Begelman 1988)). The Hot DOG SEDs are broadly similar. They have a steep red power-law IR ( $1\text{--}5 \mu\text{m}$ ) section with a potential mid-IR peak from hot dust emission, a mid-IR to submm section that appears to be flatter, i.e. less peaked, than the Polletta AGN templates, turning over to a Rayleigh-Jeans spectrum longwards of  $200 \mu\text{m}$  from the coolest dust emission. The mid-IR to submm section is consistent with being ‘‘flat-topped’’ (in  $f_\nu$ ), as suggested by Wu et al. (2012), and consistent with the  $850 \mu\text{m}$  data presented in this paper, and consistent to

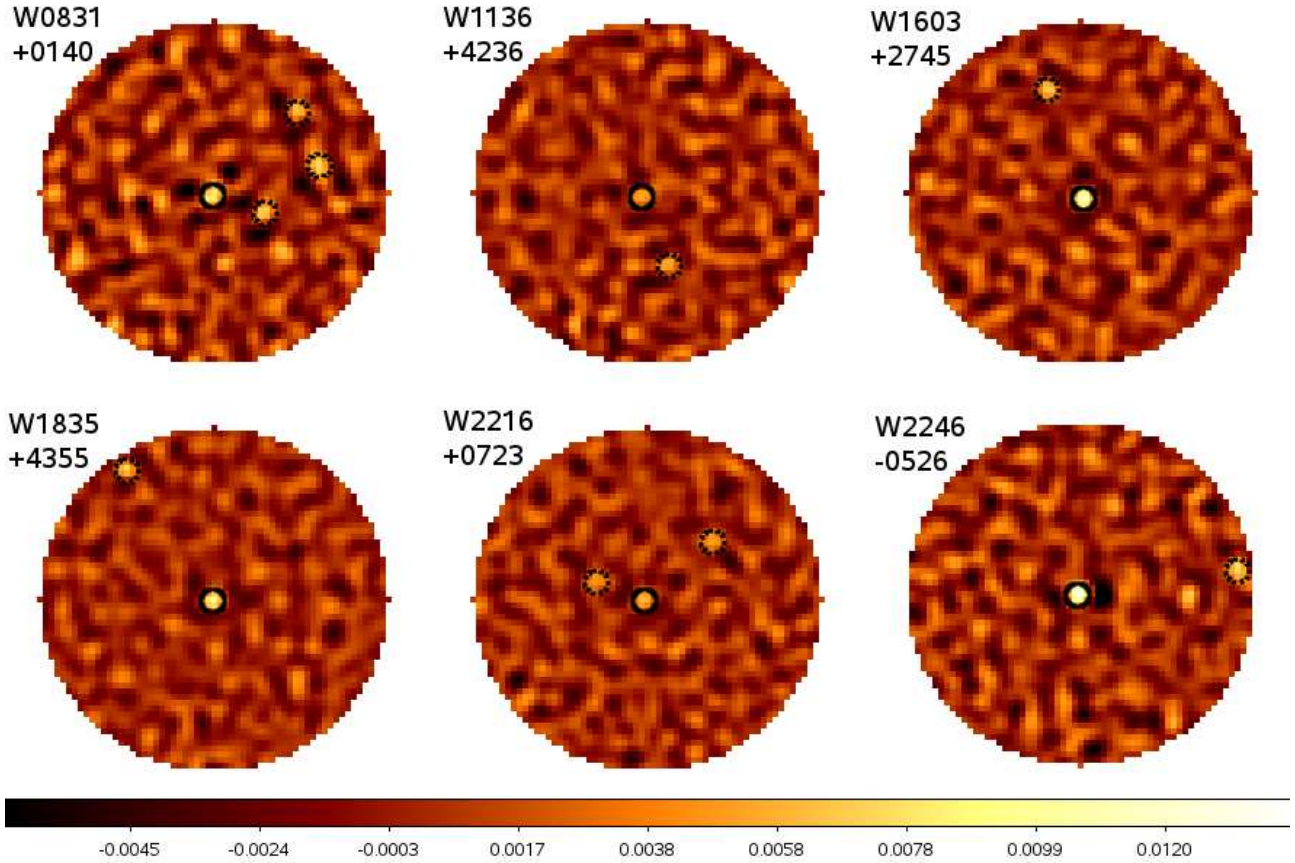


**Figure 1.** SCUBA-2 850  $\mu\text{m}$  1.5 arcmin radius maps of the 6 detected targets; W0831+0140, W1136+4236, W1603+2745, W1835+4355, W2216+0723 and W2246–0526. The solid circles show the 15-arcmin beam-sized apertures centred on the WISE RA DEC of the targets. Serendipitous sources brighter than  $3\sigma$  and within 1.5 arcmin radius of the WISE target are shown by the dotted 15-arcmin beam-sized circles. The colour flux bar at the bottom is in Jy. North is up, East is to the left.

*Herschel* results from the most luminous Hot DOGs (Tsai et al. in prep.). However, *Herschel* data of Lyman-alpha blobs (LABs) (Bridge et al. 2013) that have similar WISE colours to the Hot DOGs in this paper show a far-IR peak in the SED. Further discussion of this point and the presentation of *Herschel* follow-up of WISE Hot DOGs will be presented by Bridge et al. in prep. and Tsai et al. in prep.

A better fitting SED model for these Hot DOGs is also shown in Figure 5 and Figure 6. The W1814+3412 template shown is entirely empirical, and assumes a single-temperature dust spectrum representing the minimum dust temperature present ( $53 \pm 5\text{ K}$ ), with an emissivity index of  $\beta = 1.5$  at longer wavelengths, smoothly interpolated to a power-law spectrum instead of a Wien law at shorter wavelengths, with an opacity factor imposed at the shortest mid-IR wavelengths, to match the WISE data, corresponding to a finite total luminosity  $L_{8-1000\mu\text{m}} = 4.6 \times 10^{13} L_{\odot}$  for W1814+3412. It is constrained by *Herschel* data from Wu et al. (2012) and IRAM data from Blain et al. (in prep.), and so unsurprisingly provides a better fit than the Polletta et al. (2007) templates that pre-date these observations.

The SEDs are not well-fitted by any of the templates; the closest fitting template is the single torus template, although extra dust extinction is required to fit the W1 and W2 data. Between the Polletta torus template and

the mean SED of the 850  $\mu\text{m}$  detected targets, both normalised at 3  $\mu\text{m}$ , the extra dust extinction required at rest-frame 1  $\mu\text{m}$  is 1.6 mag. Converting to a V-band extinction implies an extra dust extinction  $A_V \geq 6.8$  mag. Eisenhardt et al. (2012) found significant obscuration in the SED of W1814+3412 with a dust extinction value of  $A_V = 48 \pm 4$  in the rest-frame from optical SED fitting. The gas column density  $N_H$  can be estimated by applying a standard “gas-to-extinction” equation  $N_H \approx 2A_V \times 10^{22} \text{ mag}^{-1} \text{ cm}^{-2}$  from Maiolino et al. (2001), which estimates the extra  $N_H$  needed is  $10^{23} \text{ cm}^{-2}$ . The Polletta torus template was modelled on a heavily obscured type-2 QSO, with a rest-frame  $N_H$  of  $2.14^{+0.54}_{-1.34} \times 10^{24} \text{ cm}^{-2}$  (Polletta et al. 2006). The extra  $N_H$  can be added to the Polletta torus template  $N_H$  to estimate the total  $N_H$  of the Hot DOGs to be  $\sim 2.3 \times 10^{24} \text{ cm}^{-2}$ , implying a Compton-thick AGN (Osterbrock & Shaw 1988; Madau et al. 1994; Comastri et al. 1995; Maiolino & Rieke 1995; Risaliti et al. 1999; Piconcelli et al. 2003; Treister & Urry 2005). This is consistent with Stern et al. (2014), who observed three Hot DOGs, including W1814+3412 in common with this paper, with NuSTAR and XMM-Newton, and found that the three targets have gas column densities  $N_H \geq 10^{24} \text{ cm}^{-2}$ , which implies the targets are Compton-thick AGNs.



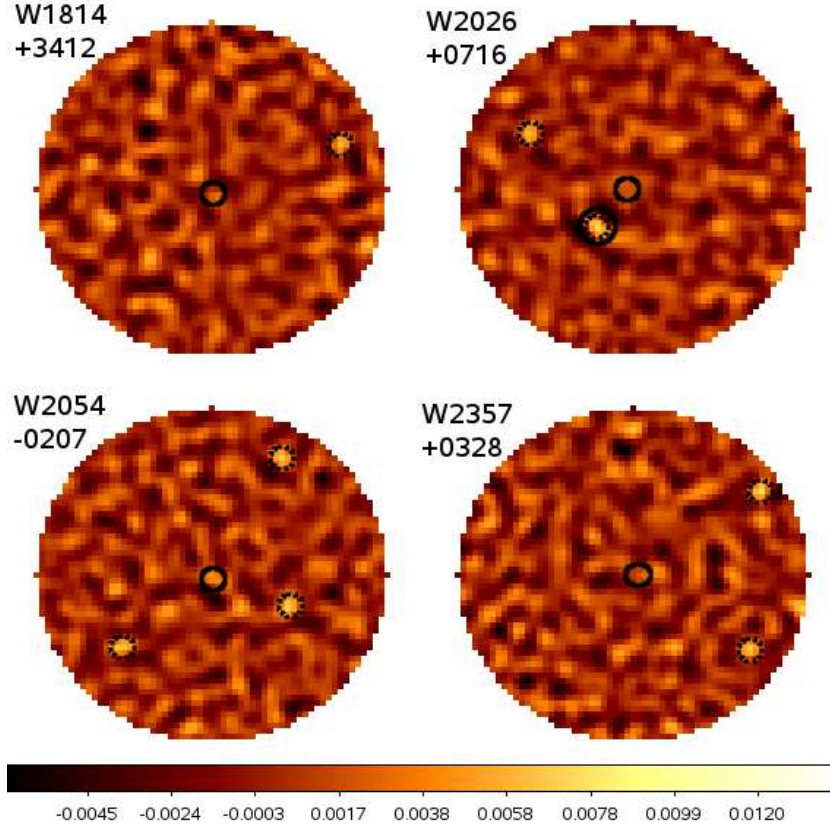


**Figure 2.** SCUBA-2 850  $\mu\text{m}$  1.5 arcmin radius maps of the 4 undetected targets; W1814+3412, W2026+0716, W2054+0207 and W2357+0328. The solid circles show the 15-arcmin beam-sized apertures centred on the WISE RA DEC of the targets. Serendipitous sources brighter than  $3\sigma$  and within 1.5 arcmin radius of the WISE target are shown by the dotted 15-arcmin beam-sized circles, and serendipitous source brighter than  $4\sigma$  is shown by the dotted 15-arcmin beam-sized circle surrounded by a solid black circle. The colour flux bar at the bottom is in Jy. North is up, East is to the left.

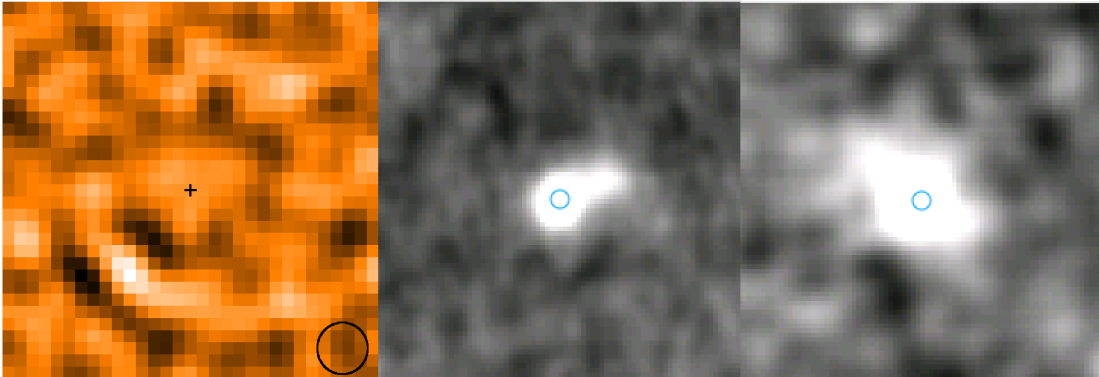


**Figure 3.** Left: The 2 arcmin  $\times$  2 arcmin SCUBA-2 850  $\mu\text{m}$  map of W2026+0716. Increasing the aperture size out to 29 arcsec in diameter increases the measured flux for this target, which could be due to multiple components of the target or to nearby, unrelated sources. The beam-size (15 arcsec diameter) is represented by the black circle. Note the  $4.4\sigma$  serendipitous source  $\sim 35$  arcsec south-east of the target. Centre and right: WISE W3 and W4 images, respectively, showing the same region of sky, with a circle showing the WISE determined position of the target. The target is not extended in the WISE images. North is up, and East is to the left.

### 3.2.2 Long Wavelength SEDs

Normalised to the WISE data at rest-frame  $3\mu\text{m}$  that lies within the WISE rest-frame wavelength range for all of our Hot DOGs, the SCUBA-2 data shows that the Hot DOGs have less submm emission than the Polletta torus template, with an average flux difference factor of 5 between the data

and template, and a range of 2-8 factor, for the detected targets, and an average flux difference factor of 7 between the data and template, and a range of 6-8, for the undetected targets (limits plus  $2\sigma$ ).

The submm to mid-IR ratio ( $F_{850\mu\text{m}} / F_{22\mu\text{m}}$ ) of the 10 targets in the observed frame are listed in Table 1. The

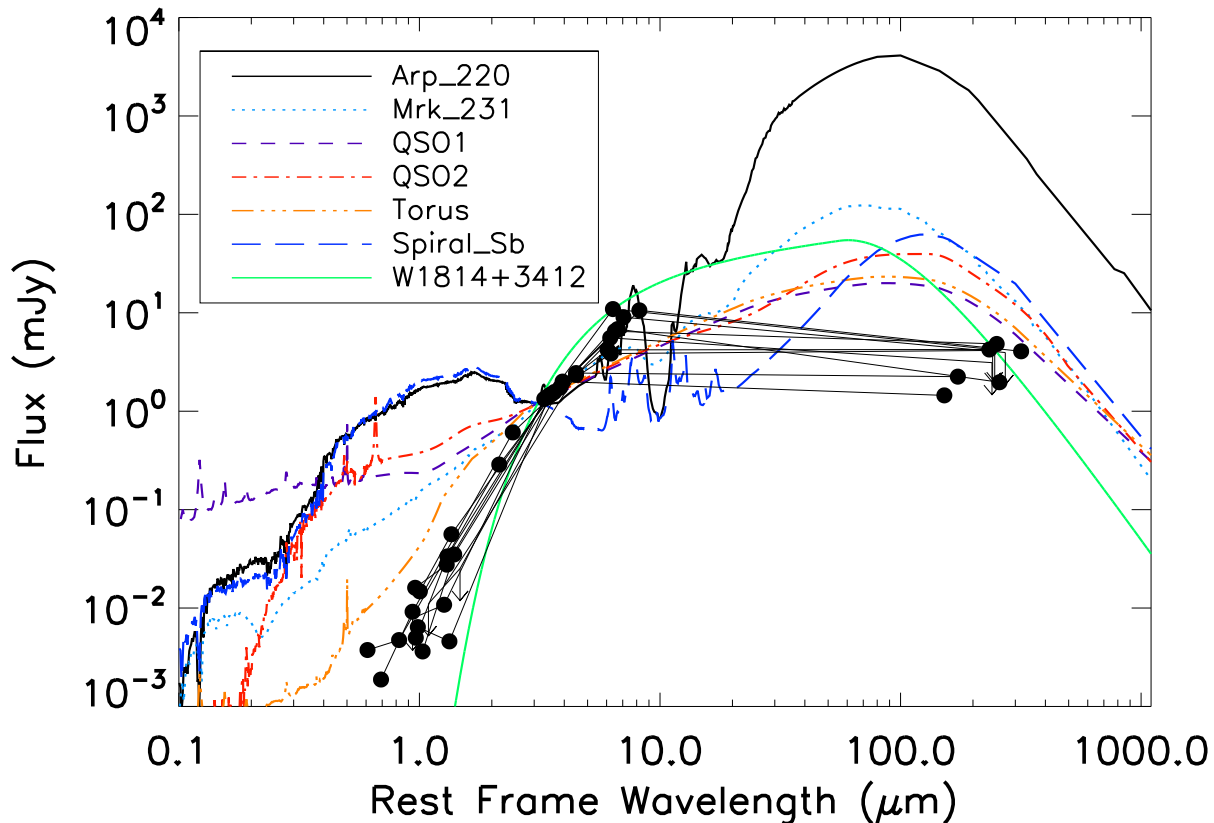


**Figure 5.** SEDs of the 10 Hot DOGs including the  $850\,\mu\text{m}$  SCUBA-2 data in rest-frame wavelengths with Arp 220, Mrk 231, QSO 1, QSO 2 and torus galaxy templates from Polletta et al. (2007) and W1814+3412 template from Blain et al. (in prep.) normalised at  $3\,\mu\text{m}$ . Detections are represented by filled circles, while  $2\sigma$  upper limits are represented by arrows. The data points for the Hot DOGs are connected for clarity, and do not represent the true SED.

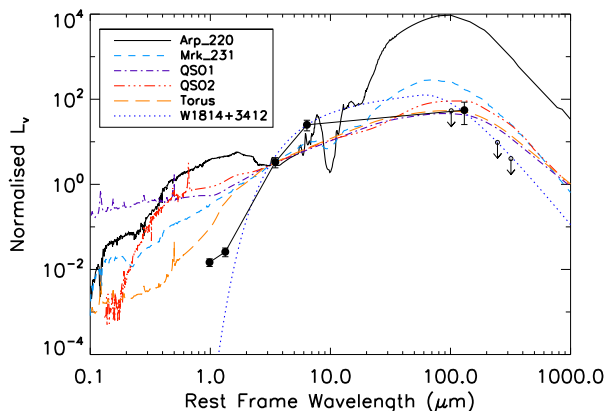


**Figure 6.** SED of W1814+3412 at  $z=2.452$ , including the  $850\,\mu\text{m}$  SCUBA-2 data with Polletta galaxy templates Arp 220, Mrk 231, QSO 1, QSO 2 and torus (Polletta et al. 2007) and W1814+3412 template (Blain et al. in prep.) normalised at rest-frame  $3\,\mu\text{m}$ . CSO SHARC-II  $350\,\mu\text{m}$  and  $450\,\mu\text{m}$  and CSO Bolocam  $1100\,\mu\text{m}$  data points from Wu et al. (2012) are included. Detections are represented by filled circles, while  $2\sigma$  upper limits are represented by arrows.

weighted average  $F_{850\,\mu\text{m}} / F_{22\,\mu\text{m}}$  of the six detected targets is  $0.6 \pm 0.1$ , where the error is the weighted standard error. Figure 7 shows these ratios in the observed sample, and for the W1814+3412 and Polletta AGN torus templates, as a function of redshift. The subsequent empirical W1814+3412 template provides a better fit to the targets, as expected. Most of the Hot DOGs appear to lie near the W1814+3412 template but show no clear sign of the expected K-correction with redshift of the templates: in particular the two highest redshift Hot DOGs (W0831+0140 and W2246–0526) lie beneath both templates with relatively faint submm fluxes, and similar observed submm to mid-IR ratios of the other lower redshift Hot DOGs. They are also the most luminous targets, with infrared luminosities,  $L_{8-1000\,\mu\text{m}} > 10^{14} L_{\odot}$  (see section 3.3), which suggests that they have hotter effective dust temperatures compared with the rest of the sample. Another distant Hot DOG, W0410-0913 at  $z = 3.592$ , was reported by Wu et al. (2012). It has a submm to mid-IR ratio of  $3.2 \pm 0.8$  ( $\log(0.5 \pm 0.1)$ ), and lies close to the W1814+3412 template.

The Hot DOGs are all consistent with high dust temperatures inferred from the submm/WISE data (Wu et al. 2012). The W1814+3412 template (Figure 6) has a temperature of  $53 \pm 5\,\text{K}$  for the coolest contribution to the

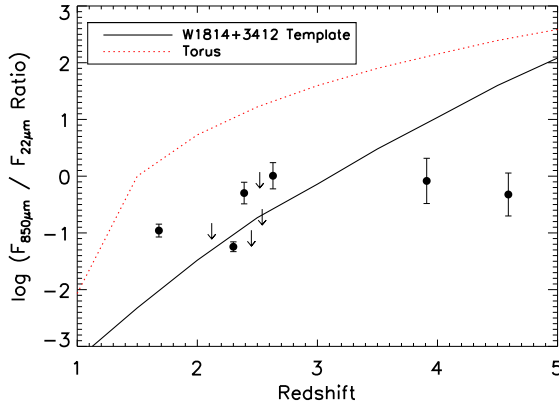


**Figure 7.** The submm to mid-IR ratio ( $F_{850\mu\text{m}} / F_{22\mu\text{m}}$ ) of the 10 Hot DOGs. The solid line shows the W1814+3412 template (Blain et al. in prep.) and the dotted line shows Polletta torus template (Polletta et al. 2007) as a function of redshift. Detections are represented by filled circles, while  $2\sigma$  upper limits are represented by arrows.

SED. Estimates of the temperatures for Hot DOGs and WISE-selected LABs have included 60-120K (Wu et al. 2012) and 40-90K (Bridge et al. 2013). This is greater than other SMGs and DOGs, which have typical temperatures of 25 - 40 K (Chapman et al. 2005; Coppin et al. 2008; Magnelli et al. 2012; Melbourne et al. 2012). The definitions of SED shape and temperature contributions can be complex, but the rest-frame peak of the Hot DOG SEDs occurs bluewards of other galaxy classes.

### 3.3 Luminosities

Total IR luminosities are calculated for each target using a minimal power-law interpolation between the WISE and SCUBA-2 data points, and also by using the W1814+3412 template with each targets' WISE and SCUBA-2 data.

A conservative lower limit to the total IR luminosities of the galaxies were estimated by connecting all the WISE and SCUBA-2 data points with power-laws and then integrating, without extrapolating beyond the range of the data in wavelength. This luminosity is a conservative estimate because any strong peak in the SED would not be included on the power-law interpolation. The resulting  $L_{8\mu\text{m}-\text{SCUBA2}}$  values for the 10 Hot DOGs are presented in Table 2. The six detected targets have values that range from  $(1.0 \pm 1.8) \times 10^{13} L_{\odot}$  to  $(1.3 \pm 2.9) \times 10^{14} L_{\odot}$ , with one having  $L_{8\mu\text{m}-\text{SCUBA2}} \geq 10^{14} L_{\odot}$ . This classifies them all as HyLIRGs.

The  $L_{8-1000\mu\text{m}}$  are also found by fitting the W1814+3412 template from Blain et al. (in prep.) with the targets' SCUBA-2 data. The W1814+3412 template was used because it is based on data from WISE, *Herschel* and IRAM of the Hot DOG W1814+3412 that are near the peak of the SED. The six detected targets assuming the W1814+3412 template, yield luminosities from  $(2.7 \pm 1.6) \times 10^{13} L_{\odot}$  to  $(6.4 \pm 2.4) \times 10^{14} L_{\odot}$ , the factor of  $\sim 4$  difference between the two methods for calculating the luminosities is due to the systematic uncertainties of the SED.

Our total IR luminosity of W1835+4355 ( $L_{8\mu\text{m}-\text{SCUBA2}} = 4.0 \pm 4.1 \times 10^{13} L_{\odot}$ ), the source also observed by CSO, is consistent with  $L_{8-1000\mu\text{m}} = 6.5 \times 10^{13} L_{\odot}$  reported in Wu et al. (2012). The derived luminosity of the W1814+3412 template from Blain et al. (in prep.) was  $L_{8-1000\mu\text{m}} = 4.6 \times 10^{13} L_{\odot}$  and compared with the luminosity calculated using the WISE and SCUBA-2 data was  $L_{8\mu\text{m}-\text{SCUBA2}} < 2.0 \times 10^{13} L_{\odot}$ , is slightly higher due to the W1814+3412 template included CSO SHARC-II data, which is nearer the peak of the SED.

Exceptionally bright galaxies can often be found to be gravitational lensed, for example Eisenhardt et al. (1996); Williams & Lewis (1996); Solomon & Vanden Bout (2005); Vieira et al. (2010); Negrello et al. (2010); Busmann et al. (2013). However, the Hot DOG luminosities are thought to be intrinsic and not due to gravitational lensing: high-resolution imaging programmes (Bridge et al. in prep.; Petty et al. in prep) from *Hubble Space Telescope* (*HST*) and ground-based telescopes of a subset of Hot DOGs show no obvious lensed structures (Wu et al. 2014). Resolved near-IR *HST* observations show the population to have a range of morphologies from clumpy and extended to point-like (Bridge et al. in prep.; Petty et al. in prep.). This suggests that the Hot DOGs are indeed amongst the most intrinsically luminous galaxies in the universe (Eisenhardt et al. 2012; Tsai et al. in prep.).

The four undetected Hot DOGs each have  $L_{8\mu\text{m}-\text{SCUBA2}} \leq 10^{13} L_{\odot}$  (Table 2). The stacked  $850\mu\text{m}$  flux density ( $7.8 \pm 2.3 \text{ mJy}$ ) of the four targets with  $850\mu\text{m}$  upper limits was used with the W1814+3412 template to estimate the luminosity  $L_{8-1000\mu\text{m}} = (9.3 \pm 4.7) \times 10^{13} L_{\odot}$ , which is consistent with a HyLIRG. A higher luminosity could be found if there are *Herschel* detections of a significant peak in the far-IR (Bridge et al. in prep.; Tsai et al. in prep.).

We also use the SCUBA-2 data to limit the luminosity of an underlying extended galaxy. A spiral (Sb) galaxy template and a warmer ULIRG-type (Arp 220) template were fitted to account for all of the SCUBA-2  $850\mu\text{m}$  flux density, and then by integrating under the Sb or Arp 220 template, the maximum total luminosity of this template SED can be estimated. This approach assumes that an underlying extended dusty galaxy, disconnected from the mid-IR emission, accounts for all of the measured SCUBA-2 flux. This extended emission can be assumed to all be due to star-formation rather than an AGN. An Sb host galaxy template cannot exceed  $\sim 2\%$  of the inferred Hot DOG luminosity from 8-1000  $\mu\text{m}$ . This would give a Sb luminosity of  $1.3 \times 10^{12} L_{\odot}$ ; 22 times more luminous than the Milky Way ( $6 \times 10^{10} L_{\odot}$ ), with an equivalent star formation rate (SFR) of  $\sim 30 M_{\odot} \text{ yr}^{-1}$ , which is lower than the UV-derived SFR of  $\sim 300 M_{\odot} \text{ yr}^{-1}$  derived for W1814+3412 (Eisenhardt et al. 2012). An Arp 220 ULIRG template can account for the  $850\mu\text{m}$  data, if the host galaxy has a luminosity of  $2.9 \times 10^{13} L_{\odot}$ ,  $\sim 55\%$  of the inferred Hot DOG luminosity, with an equivalent SFR of  $\sim 450 M_{\odot} \text{ yr}^{-1}$ . This emphasises that the full Hot DOG SED from 8-1000  $\mu\text{m}$  has a small contribution from cold far-IR dust and is dominated by hot dust and mid-IR emission.



### 3.4 Clustering

There is significant evidence from previous studies that the galaxy density in the environments of high-redshift far-IR and mid-IR luminous galaxies and SMGs appears to be above average (Scott et al. 2002; Blain et al. 2004; Borys et al. 2004; Scott et al. 2006; Farrah et al. 2006; Gilli et al. 2007; Chapman et al. 2009; Cooray et al. 2010; Hickox et al. 2012). Clustering of SMGs could be evidence of massive dark matter halos associated with the SMGs at high-redshift. To investigate if there is clustering of SMGs in the Hot DOG fields, the serendipitous sources number counts will be compared with the number counts from two different blank-field submm surveys. To provide another way to test SMG clustering in the Hot DOG fields, 1.5-arcmin-radius circles will be placed at random and centred on SMG detections in a blank-field submm survey.

Seventeen serendipitous 850  $\mu\text{m}$  sources were detected at greater than  $3\sigma$  in the 10 SCUBA-2 maps, and one source was detected at greater than  $4\sigma$ ; see Table 3. The total area surveyed is 71  $\text{arcmin}^2$ , or about 1500 SCUBA-2 850  $\mu\text{m}$  beams. Figure 1 and Figure 2 show the location of detected serendipitous sources in the SCUBA-2 fields of all the detected and undetected Hot DOGs, respectively.

There are  $4 \pm 2$  negative peaks in the 10 maps at above the same  $3\sigma$  threshold (see Table 3), consistent with the  $2 \pm 1$   $3\sigma$  negative peaks expected from Gaussian noise.

To see if there is evidence for an over-density of SMGs in the 10 SCUBA-2 Hot DOG fields, the number of serendipitous sources can be compared with the results of field submm surveys. In the LESS survey, Weiß et al. (2009) detected 126 SMGs in a uniform area of 1260  $\text{arcmin}^2$  with a noise level of 1.2 mJy at 870  $\mu\text{m}$ . They also found evidence for an angular two-point clustering signal on angular scales smaller than 1 arcmin. There are 101 LESS sources brighter than our average  $3\sigma$  flux density limit of 5.3 mJy, which implies 5.7 serendipitous sources would be expected in our 10 SCUBA-2 fields; however, we find 15. This indicates a relative overdensity of SMGs in our Hot DOG fields by a factor of  $2.6 \pm 0.7$ . The noise level range of our maps is 1.5–2.1 mJy  $\text{beam}^{-1}$ . In order to check the effect of our range of sensitivity in each field we also compare the number of SMGs at our highest noise level (2.1 mJy  $\text{beam}^{-1}$ ) with to the LESS survey. The number of LESS sources brighter than our greatest  $3\sigma$  flux density limit of 6.3 mJy is 60 SMGs, which implies that 3.4 serendipitous sources would be expected in our 10 SCUBA-2 fields. However, we find 9 and thus a relative overdensity of SMGs by a factor of  $2.7 \pm 1.0$ . The overdensity using the highest noise level is consistent with that using the average noise level; therefore, the difference in the 10 map noise levels appears not to have a large effect on the overdensity factor.

A complementary way to test whether there is an overdensity of SMGs near the Hot DOG targets is to place 1.5-arcmin-radius circles at random locations in the LESS field and count the number of sources from the catalogue source positions that would have been detected in our survey, taking into account the differences in depth, by employing a flux density limit of 5.3 mJy. The 1.5-arcmin-radius circles were chosen because the SCUBA-2 maps were 1.5 arcmin in radius. In 10 sets of 10 randomly selected 1.5-arcmin-radius circles within LESS, we found  $7 \pm 3$  LESS sources

brighter than 5.3 mJy, to mimic our SCUBA-2 images in this surveyed field. The total number of 1.5-arcmin-radius fields available within LESS is  $\sim 200$ . There is thus a hint of evidence for a relative over-density of SMGs around Hot DOGs by a factor of  $2.1 \pm 1.0$  as compared with this blank-field.

A third way to test the over density of SMGs in the SCUBA-2 fields is to compare the number of LESS sources brighter than 5.3 mJy within 1.5-arcmin-radius circles centred on LESS-detected sources. In 101 available positions, there are 18 not counting the LESS sources on which each 1.5-arcmin-radius field was centred. This suggests that in 10 SCUBA-2 fields centred on LESS detections there would be only 1.8 serendipitous sources detected; however, we find 15 centred on WISE-selected targets, potentially giving a Hot DOG to SMG companion overdensity factor of order 8.

We can repeat this approach in another submm blank-field survey. Casey et al. (2013) used SCUBA-2 to observe the COSMOS field over a uniform area of 394  $\text{arcmin}^2$  at a noise level of 0.80 mJy at 850  $\mu\text{m}$  and detected 99 SMGs brighter than  $3.6\sigma$ . There are 18 COSMOS sources brighter than our average detection threshold of 5.3 mJy ( $3\sigma$ ), which would imply 6.3 serendipitous sources expected in the 10 SCUBA-2 Hot DOG fields. We find 15, implying a relative overdensity of SMGs by a factor of  $2.4 \pm 0.7$ , which is consistent with  $2.6 \pm 0.7$  from LESS. The number of sources brighter than our greatest  $3\sigma$  flux density limit of 6.3 mJy is 18 SMGs, which implies that 3.2 serendipitous sources would be expected in our 10 SCUBA-2 fields. However, we find 9 and thus a relative overdensity of SMGs by a factor of  $2.8 \pm 1.1$ , which is consistent with  $2.7 \pm 1.0$  from LESS. Again, the variation in noise levels of the 10 Hot DOG field does not appear to have a large effect on the overdensity factor. These results are consistent with the LESS survey. Random 1.5-arcmin-radius circles were not placed in the COSMOS field due to the small size of the field, with only  $\sim 50$  1.5-arcmin-radius fields available.

The six detected Hot DOG targets and the four undetected Hot DOG targets have similar numbers of serendipitous sources, see Figure 1 and Figure 2. The overdensity of SMGs around detected and undetected Hot DOGs appear to be comparable.

Figure 8 shows the fraction of the total number of serendipitous sources for the 10 SCUBA-2 maps found within 0.25, 0.5, 0.75, 1.0, 1.25 and 1.5 arcmin from the WISE target. The expected fraction of the total number of serendipitous sources with no angular clustering is also plotted on Figure 8. There is no hint of angular clustering of serendipitous sources around the Hot DOGs on these scales, despite the greater average density of submm sources in the WISE fields as compared with blank-field surveys. Clustering of SMGs on larger scales could be expected because there is tentative evidence of clustering from previous submm studies on scales up to  $\sim 8$  arcmin (Scoville et al. 2000; Blain et al. 2004; Greve et al. 2004; Farrah et al. 2006; Ivison et al. 2007; Weiß et al. 2009; Cooray et al. 2010; Scott et al. 2010; Hickox et al. 2012). Nevertheless, the lack of a clear two-point correlation signal is interesting, because SMG clustering observations can constrain the nature of the host halos around SMGs (Cooray et al. 2010).

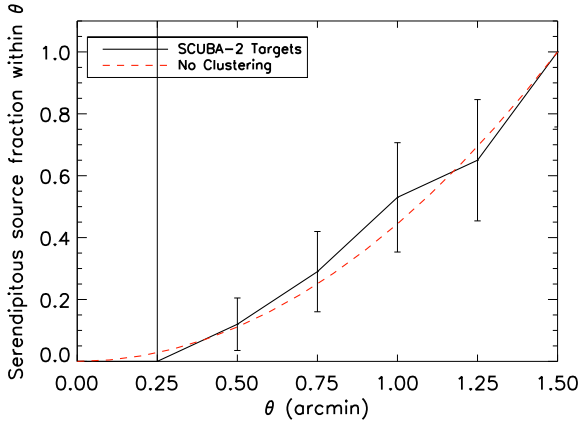


**Figure 8.** The fraction of the total number of serendipitous sources in each field within different radii of the WISE targets. The solid line shows the fields of the Hot DOGs. The dashed-dotted line shows the expected number of serendipitous sources if they are randomly located with no clustering. The beam size of SCUBA-2 at  $850\,\mu\text{m}$  is  $14.5\,\text{arcsec}$ ; serendipitous sources cannot be detected within the beam.

#### 4 DISCUSSION

The above results obtained for the Hot DOGs will be discussed by comparing their SEDs and luminosities with other galaxy populations. Next the Hot DOGs environments are investigated by comparing the serendipitous source number counts to other submm surveys.

The Hot DOG SEDs in Figure 5 show a blue mid-IR to submm colour. A Compton-thick AGN torus template would fit the Hot DOG SEDs if extra mid-IR extinction of  $A_V \geq 6.8\,\text{mag}$  is included. These results can be compared with the SEDs of ULIRGs and LIRGs which have large amounts of obscuring material around the AGN and/or starburst activity, and have estimated dust extinctions between  $A_V \simeq 5$  and  $50\,\text{mag}$  (Genzel et al. 1998). Comparing the SED of Arp 220 (a starburst-dominated ULIRG) with the Hot DOG SEDs in Figure 5, reveals that the Hot DOGs appear to have more mid-IR dust extinction than the exceptionally mid-IR red Arp 220. This leads to the conclusion that the Hot DOGs have extremely large amounts of absorption in the AGN torus, and/or host galaxy (Goulding et al. 2012), and could have even larger amounts of obscuring material than typical ULIRGs and LIRGs.

The SCUBA-2 observations show that the Hot DOGs have relatively less submm emission than other galaxy SED templates: the detected Hot DOG targets' SCUBA-2 flux density is on average 5 times fainter than the Polletta torus template. This leads to the suggestion that the Hot DOGs have less cold dust in the host galaxy and/or on the outer edge of the torus, and hence the torus could be denser, smaller and hotter than in the template. Alternatively, less submm emission could be due to an excess of mid-IR emission from the AGN as compared with the torus template (Wu et al. 2012). The median  $850\,\mu\text{m}$  flux density of SMGs,  $5.7 \pm 3.0\,\text{mJy}$  (Chapman et al. 2005), is comparable with these Hot DOGs with a median  $850\,\mu\text{m}$  flux density of  $5.4 \pm 1.8\,\text{mJy}$ . Since SMGs and Hot DOGs have similar redshifts ( $z \sim 2$ ), this might suggest comparable cold dust properties.

However, to address the degree of similarity between SMGs and Hot DOGs in the far-IR will require knowledge of the far-IR colours of Hot DOGs with data from *Herschel* (Bridge et al. in prep.; Tsai et al. in prep.).

The luminosities of all six detected targets (with a mean luminosity of  $L_{8\mu\text{m}-\text{SCUBA2}} = 5.3 \times 10^{13}\,L_\odot$  and a median luminosity of  $L_{8\mu\text{m}-\text{SCUBA2}} = 3.6 \times 10^{13}\,L_\odot$ ) are greater than those of typical SMGs, which have  $L_{8-1000\mu\text{m}} = 8.5 \times 10^{12}\,L_\odot$  (Chapman et al. 2005; Kovács et al. 2006), and DOGs, which have a mean luminosity  $L_{8-1000\mu\text{m}} = 9 \times 10^{12}\,L_\odot$  (Melbourne et al. 2012). This is in agreement with Wu et al. (2012) who found a sample mean  $L_{8-1000\mu\text{m}} = 6.1 \times 10^{13}\,L_\odot$  for Hot DOGs. However, the targets in this paper and Wu et al. (2012) could be biased towards being the mid-IR brightest and rarest galaxies, because they were selected on the grounds of their bright mid-IR flux. It is certainly inevitable that deeper mid-IR samples will include DOGs and SMGs; however, our current observed sample of 10, which has a range of W4 fluxes (6.19 to 7.66 mag, or 7.2 to 27.7 mJy), due to the various selection cuts involved, certainly shows no SMG/ULIRG type SEDs. Eight WISE-selected LABs (Bridge et al. 2013) were also found to be ultra-luminous galaxies from *Herschel* data ( $L_{8-1000\mu\text{m}} = 2.3 \times 10^{13}\,L_\odot$ ), and included a wider range of mid-IR fluxes with no colour cut, again indicating very luminous mid-IR properties of galaxies with extremely red WISE colours.

Comparing number counts of the serendipitous sources in the 10 Hot DOG fields with other submm surveys, implies there is an overdensity of SMGs in the 10 SCUBA-2 fields by factor of  $\sim 2$ -3. This is consistent with finding Hot DOGs in potentially overdense environments. Umehata et al. (2014) observed the protocluster SSA22 field with the Astronomical Thermal Emission Camera (AzTEC) on the Atacama Submillimeter Telescope Experiment (ASTE), at  $1.1\,\text{mm}$  to a depth of  $0.7 - 1.3\,\text{mJy beam}^{-1}$ , and found 10 SMGs are correlated with  $z = 3.1$  Lyman-alpha emitters (LAE)s in the protocluster, which suggests that SMGs are formed in dense environments. Our SMG overdensity around Hot DOGs could indicate that Hot DOGs signpost protocluster regions.

These Hot DOGs appear to be very powerful AGN that have more mid-IR emission and mid-IR opacity than AGN in standard galaxy templates. Therefore, the Hot DOGs might be experiencing the most powerful feedback possible and could be an AGN-dominated short evolutionary phase of merging galaxies, and appear to reside in intriguing arcmin-scale overdensities of very luminous, dusty sources.

#### 5 SUMMARY

The results from SCUBA-2  $850\,\mu\text{m}$  observations of 10 WISE-selected, high-redshift, luminous, dusty Hot DOGs are:

- The 10 Hot DOGs have SEDs that are not well fitted by the current AGN templates (see Figure 5). The best fitting single Polletta torus template (Polletta et al. 2007) needs extra dust extinction to fit the Hot DOG SEDs with extra  $A_V \geq 6.8\,\text{mag}$ , which could be due to more screening from the host galaxy and/or AGN torus. The  $N_H$  was estimated to be  $\sim 2.3 \times 10^{24}\,\text{cm}^{-2}$ , which is Compton-thick.
- The Hot DOGs have a lower ratio of cold to hot dust than the Polletta torus template, which could be because

there is less cold dust in the host galaxy, and/or the outer AGN torus in the Hot DOGs are smaller. Alternatively there could be more intense mid-IR emission from the inner regions (Wu et al. 2012). *Herschel* observations near the peak of the SED should soon provide more information.

- Despite being observed over a wide redshift range, the Hot DOGs show uniform submm to mid-IR ratios. The highest redshift, most luminous targets, could thus have hotter dust temperatures than assumed in the templates. However, the number of targets involved is currently only modest and the selection of the targets is sensitive to redshift, owing to very red intense WISE colours.

- The six SCUBA-2 detected Hot DOGs have very high IR luminosities,  $L_{8\mu\text{m}-\text{SCUBA2}} \geq 10^{13} L_{\odot}$ : they are HyLIRGs. These are conservative values as any pronounced peak of the SED would increase these further and could be missed without *Herschel* data. The stacked IR luminosity,  $L_{8-1000\mu\text{m}} = (9.3 \pm 4.7) \times 10^{13} L_{\odot}$ , of the four undetected targets is consistent with being a HyLIRG. With no obvious signatures of gravitational lensing known, Hot DOGs are amongst the most luminous galaxies.

- The luminosity of an underlying extended star-forming galaxy cannot exceed a luminosity  $\sim 2\%$  (for a cool spiral galaxy template) or  $\sim 55\%$  (for a warmer ULIRG-like galaxy template) as compared with the typical Hot DOG luminosity, respectively. Our SCUBA-2 observations confirm that Hot DOGs are a mid-IR dominated population.

- When comparing the submm galaxy counts of the 10 1.5-arcmin-radius SCUBA-2 maps observed here to blank-field surveys, there is an over-density of SMGs on this scale by a factor 3, but no evidence for any angular clustering within these fields.

- The next step to understand these Hot DOGs is with more *Herschel* observations to accurately define the peak of the SED and increase the sample size, presented in future papers (Bridge et al. in prep.; Tsai et al. in prep.). Another subpopulation of galaxies selected with similar WISE colours but also selected to be radio bright, that could be AGN quenching star formation by radio jet feedback at the highest rate of AGN fueling. A larger number of these targets have been observed with SCUBA-2 and Atacama Large Millimeter/submillimeter Array (ALMA), and will be presented in future papers (Jones et al. in prep.; Lonsdale et al. in prep.). These SCUBA-2 observations provide a comparable density analysis.

## 6 ACKNOWLEDGEMENTS

The authors would like to thank the anonymous referee for his/her comments and suggestions, which have greatly improved this paper.

S. F. Jones gratefully acknowledges support from the University of Leicester Physics & Astronomy Department. R. J. Assef was supported by Gemini-CONICYT grant number 32120009. This publication makes use of data products from the *Wide-field Infrared Survey Explorer*, which is a joint project of the University of California, Los Angeles, and the Jet Propulsion Laboratory/California Institute of Technology, funded by the National Aeronautics and Space Administration.

The James Clerk Maxwell Telescope is operated by

the Joint Astronomy Centre on behalf of the Science and Technology Facilities Council of the United Kingdom, the Netherlands Organisation for Scientific Research, and the National Research Council of Canada. Additional funds for the construction of SCUBA-2 were provided by the Canada Foundation for Innovation. The program ID under which the data were obtained was M12AU010.

## REFERENCES

- Barnes J. E., Hernquist L., 1992, *ARA&A*, 30, 705  
 Blain A. W., Chapman S. C., Smail I., Ivison R., 2004, *ApJ*, 611, 725  
 Blain A. W., Smail I., Ivison R. J., Kneib J.-P., 1999, *MNRAS*, 302, 632  
 Blain A. W., Smail I., Ivison R. J., Kneib J.-P., Frayer D. T., 2002, *Phys. Rep.*, 369, 111  
 Borys C., Scott D., Chapman S., Halpern M., Nandra K., Pope A., 2004, *MNRAS*, 355, 485  
 Bridge C. R. et al., 2013, *ApJ*, 769, 91  
 Bussmann R. S. et al., 2009, *ApJ*, 705, 184  
 Bussmann R. S. et al., 2013, *ApJ*, 779, 25  
 Casey C. M. et al., 2012, *ApJ*, 761, 140  
 Casey C. M. et al., 2013, *MNRAS*, 436, 1919  
 Chapin E. L., Berry D. S., Gibb A. G., Jenness T., Scott D., Tilanus R. P. J., Economou F., Holland W. S., 2013, *MNRAS*, 430, 2545  
 Chapman S. C., Blain A., Iyata R., Ivison R. J., Smail I., Morrison G., 2009, *ApJ*, 691, 560  
 Chapman S. C., Blain A. W., Smail I., Ivison R. J., 2005, *ApJ*, 622, 772  
 Comastri A., Setti G., Zamorani G., Hasinger G., 1995, *A&A*, 296, 1  
 Cooray A. et al., 2010, *A&A*, 518, L22  
 Coppin K. et al., 2008, *MNRAS*, 384, 1597  
 Cowie L. L., Barger A. J., Kneib J.-P., 2002, *AJ*, 123, 2197  
 Cutri R. M., et al., 2012, *VizieR Online Data Catalog*, 2311, 0  
 Dempsey J. T. et al., 2013, *MNRAS*, 430, 2534  
 Dey A. et al., 2008, *ApJ*, 677, 943  
 Eisenhardt P. R., Armus L., Hogg D. W., Soifer B. T., Neugebauer G., Werner M. W., 1996, *ApJ*, 461, 72  
 Eisenhardt P. R. M. et al., 2012, *ApJ*, 755, 173  
 Elbaz D. et al., 2011, *A&A*, 533, A119  
 Farrah D. et al., 2006, *ApJ*, 641, L17  
 Farrah D. et al., 2001, *MNRAS*, 326, 1333  
 Farrah D. et al., 2012, *ApJ*, 745, 178  
 Genzel R., Cesarsky C. J., 2000, *ARA&A*, 38, 761  
 Genzel R. et al., 1998, *ApJ*, 498, 579  
 Gilli R., Comastri A., Hasinger G., 2007, *A&A*, 463, 79  
 Goulding A. D., Alexander D. M., Bauer F. E., Forman W. R., Hickox R. C., Jones C., Mullaney J. R., Trichas M., 2012, *ApJ*, 755, 5  
 Greve T. R., Ivison R. J., Bertoldi F., Stevens J. A., Dunlop J. S., Lutz D., Carilli C. L., 2004, *MNRAS*, 354, 779  
 Hickox R. C. et al., 2012, *MNRAS*, 421, 284  
 Hinshaw G. et al., 2009, *ApJS*, 180, 225  
 Holland W. S. et al., 2013, *MNRAS*, 430, 2513  
 Hopkins P. F., Hernquist L., Cox T. J., Di Matteo T., Robertson B., Springel V., 2006, *ApJS*, 163, 1

- Hopkins P. F., Hernquist L., Cox T. J., Kereš D., 2008, *ApJS*, 175, 356
- Houck J. R. et al., 1984, *ApJ*, 278, L63
- Ivison R. J. et al., 2007, *MNRAS*, 380, 199
- Jarrett T. H. et al., 2011, *ApJ*, 735, 112
- Kovács A., Chapman S. C., Dowell C. D., Blain A. W., Ivison R. J., Smail I., Phillips T. G., 2006, *ApJ*, 650, 592
- Krolik J. H., Begelman M. C., 1988, *ApJ*, 329, 702
- Le Floch E. et al., 2005a, *ApJ*, 632, 169
- Le Floch E. et al., 2005b, *ApJ*, 632, 169
- Lonsdale C. J., Farrah D., Smith H. E., 2006, *Ultraluminous Infrared Galaxies*, Springer Verlag, p. 285
- Lu N., Zhao Y., Xu C. K., Gao Y., GOALS FTS Team, 2013, in *IAU Symposium*, Vol. 292, *IAU Symposium*, Wong T., Ott J., eds., pp. 249–249
- Madau P., Ghisellini G., Fabian A. C., 1994, *MNRAS*, 270, L17
- Magnelli B., Elbaz D., Chary R. R., Dickinson M., Le Borgne D., Frayer D. T., Willmer C. N. A., 2009, *A&A*, 496, 57
- Magnelli B. et al., 2012, *A&A*, 539, A155
- Maiolino R., Marconi A., Salvati M., Risaliti G., Severgnini P., Oliva E., La Franca F., Vanzì L., 2001, *A&A*, 365, 28
- Maiolino R., Rieke G. H., 1995, *ApJ*, 454, 95
- Melbourne J. et al., 2012, *AJ*, 143, 125
- Mihos C., 1996, in *Encyclopedia of Astronomy and Astrophysics*, IOP Publishing Ltd
- Narayanan D. et al., 2010, *MNRAS*, 407, 1701
- Negrello M. et al., 2010, *Science*, 330, 800
- Neugebauer G. et al., 1984, *ApJ*, 278, L1
- Osterbrock D. E., Shaw R. A., 1988, *ApJ*, 327, 89
- Piconcelli E., Cappi M., Bassani L., Di Cocco G., Dadina M., 2003, *A&A*, 412, 689
- Polletta M. et al., 2007, *ApJ*, 663, 81
- Polletta M. d. C. et al., 2006, *ApJ*, 642, 673
- Reddy N. A., Steidel C. C., Pettini M., Adelberger K. L., Shapley A. E., Erb D. K., Dickinson M., 2008, *ApJS*, 175, 48
- Richards G. T. et al., 2006, *AJ*, 131, 2766
- Risaliti G., Maiolino R., Salvati M., 1999, *ApJ*, 522, 157
- Sanders D. B., Mirabel I. F., 1996, *ARA&A*, 34, 749
- Sanders D. B., Soifer B. T., Elias J. H., Madore B. F., Matthews K., Neugebauer G., Scoville N. Z., 1988a, *ApJ*, 325, 74
- Sanders D. B., Soifer B. T., Elias J. H., Neugebauer G., Matthews K., 1988b, *ApJ*, 328, L35
- Schweizer F., 1998, in *Saas-Fee Advanced Course 26: Galaxies: Interactions and Induced Star Formation*, Kenicutt Jr. R. C., Schweizer F., Barnes J. E., Friedli D., Martinet L., Pfenniger D., eds., p. 105
- Scott K. S. et al., 2010, *MNRAS*, 405, 2260
- Scott S. E., Dunlop J. S., Serjeant S., 2006, *MNRAS*, 370, 1057
- Scott S. E. et al., 2002, *MNRAS*, 331, 817
- Scoville N. Z. et al., 2000, *AJ*, 119, 991
- Smail I., Ivison R. J., Blain A. W., 1997, *ApJ*, 490, L5
- Soifer B. T. et al., 1984, *ApJ*, 278, L71
- Solomon P. M., Vanden Bout P. A., 2005, *ARA&A*, 43, 677
- Spoon H. W. W. et al., 2013, *ApJ*, 775, 127
- Stern D. et al., 2014, *ArXiv e-prints*
- Tacconi L. J. et al., 2008, *ApJ*, 680, 246
- Treister E., Urry C. M., 2005, *ApJ*, 630, 115
- Tyler K. D. et al., 2009, *ApJ*, 691, 1846
- Umehata H. et al., 2014, *MNRAS*, 440, 3462
- Veilleux S., Kim D.-C., Sanders D. B., 2002, *ApJS*, 143, 315
- Vieira J. D. et al., 2010, *ApJ*, 719, 763
- Weiß A. et al., 2009, *ApJ*, 707, 1201
- Williams L. L. R., Lewis G. F., 1996, *MNRAS*, 281, L35
- Wright E. L. et al., 2010, *AJ*, 140, 1868
- Wu J. et al., 2014, *ArXiv 1405.1147*
- Wu J. et al., 2012, *ApJ*, 756, 96

**Table 1.** Coordinates and photometry of the 10 Hot DOGs, with  $3.4\,\mu\text{m}$ ,  $4.6\,\mu\text{m}$ ,  $12\,\mu\text{m}$  and  $22\,\mu\text{m}$  magnitudes from the AllWISE Source Catalog and  $850\,\mu\text{m}$  flux densities from SCUBA-2. The top six targets are detected at  $850\,\mu\text{m}$ , while the bottom four targets have upper limits at  $850\,\mu\text{m}$ . The targets with WISE upper limits have  $\text{SNR} < 2$  and therefore in the AllWISE Source Catalog the magnitudes quoted are  $2\sigma$  upper limits. For redshifts of the targets refer to Eisenhardt et al. (2012, in prep.) and Bridge et al. in prep.

Source	R.A. (J2000)	Dec. (J2000)	$3.4\,\mu\text{m}$ (mag)	$4.6\,\mu\text{m}$ (mag)	$12\,\mu\text{m}$ (mag)	$22\,\mu\text{m}$ (mag)	$850\,\mu\text{m}$ (mJy)	$850\,\mu\text{m} / 22\,\mu\text{m}$ Ratio	Redshift
W0831+0140	08:31:53.30	+01:40:10.8	$17.92 \pm 0.28$	$16.10 \pm 0.20$	$10.15 \pm 0.07$	$7.28 \pm 0.12$	$9.3 \pm 2.1$	$0.9 \pm 0.2$	3.91
W1136+4236	11:36:34.31	+42:36:02.6	$18.19 \pm 0.24$	$15.83 \pm 0.11$	$10.62 \pm 0.07$	$7.66 \pm 0.11$	$5.3 \pm 1.7$	$0.7 \pm 0.1$	2.39
W1603+2745	16:03:57.40	+27:45:53.3	$< 18.02$	$17.04 \pm 0.34$	$9.89 \pm 0.04$	$7.28 \pm 0.11$	$10.2 \pm 1.8$	$1.0 \pm 0.2$	2.63
W1835+4355	18:35:33.73	+43:55:48.7	$17.44 \pm 0.09$	$15.20 \pm 0.05$	$9.15 \pm 0.03$	$6.19 \pm 0.04$	$8.0 \pm 1.5$	$0.3 \pm 0.1$	2.30
W2216+0723	22:16:19.09	+07:23:54.5	$17.33 \pm 0.16$	$15.59 \pm 0.13$	$9.91 \pm 0.05$	$6.91 \pm 0.09$	$5.5 \pm 1.6$	$0.4 \pm 0.1$	1.68
W2246-0526	22:46:07.54	-05:26:35.1	$17.54 \pm 0.21$	$16.65 \pm 0.37$	$10.27 \pm 0.09$	$6.80 \pm 0.11$	$11.4 \pm 2.1$	$0.7 \pm 0.1$	4.59
W1814+3412	18:14:17.31	+34:12:24.8	$18.86 \pm 0.44$	$17.61 \pm 0.49$	$10.41 \pm 0.06$	$6.86 \pm 0.07$	$2.0 \pm 1.8$	$< 0.4$	2.45
W2026+0716	20:26:15.27	+07:16:23.9	$17.58 \pm 0.21$	$15.69 \pm 0.13$	$10.18 \pm 0.07$	$7.31 \pm 0.11$	$2.0 \pm 1.7$	$< 0.6$	2.54
W2054+0207	20:54:25.69	+02:07:11.0	$18.27 \pm 0.32$	$15.32 \pm 0.09$	$9.59 \pm 0.05$	$7.13 \pm 0.09$	$3.3 \pm 1.8$	$< 1.1$	2.52
W2357+0328	23:57:10.82	+03:28:03.4	$< 18.14$	$< 16.61$	$10.09 \pm 0.07$	$6.94 \pm 0.11$	$2.2 \pm 1.9$	$< 0.4$	2.12

**Table 2.** The total IR luminosities ( $8\,\mu\text{m} - \text{SCUBA2}$ ) of the 10 Hot DOGs derived by connecting all the WISE and SCUBA-2 data points with power laws and then integrating. The top six have detections at  $850\,\mu\text{m}$  and the bottom four have  $2\sigma$  upper limits at  $850\,\mu\text{m}$ . The luminosities are shown in solar luminosities,  $3.84 \times 10^{26}$  W. The W1814+3412 template total IR luminosities  $L_{8-1000\,\mu\text{m}}$  are found by using the Blain et al. (in prep.) W1814+3412 template with the Hot DOGs' SCUBA-2 data. The total IR luminosities ( $8-1000\,\mu\text{m}$ ) of two targets also observed by Wu et al. (2012) are  $4.0 \times 10^{13} L_{\odot}$  for W1814+3412, and  $6.5 \times 10^{13} L_{\odot}$  for W1835+4355, are consistent with the luminosities in the table below.

Source	Total IR Luminosities ( $8\,\mu\text{m} - \text{SCUBA2}$ ) ( $L_{\odot}$ )	W1814+3412 Template Total IR Luminosities ( $8-1000\,\mu\text{m}$ ) ( $L_{\odot}$ )
W0831+0140	$8.7 \pm 1.8 \times 10^{13}$	$3.6 \pm 1.6 \times 10^{14}$
W1136+4236	$1.5 \pm 4.6 \times 10^{13}$	$6.2 \pm 3.8 \times 10^{13}$
W1603+2745	$3.1 \pm 0.7 \times 10^{13}$	$1.5 \pm 0.5 \times 10^{14}$
W1835+4355	$4.3 \pm 4.1 \times 10^{13}$	$8.5 \pm 3.4 \times 10^{13}$
W2216+0723	$1.0 \pm 1.8 \times 10^{13}$	$2.7 \pm 1.6 \times 10^{13}$
W2246-0526	$1.3 \pm 2.9 \times 10^{14}$	$6.4 \pm 2.4 \times 10^{14}$
W1814+3412	$< 2.5 \times 10^{13}$	$< 7.0 \times 10^{13}$
W2026+0716	$< 2.1 \times 10^{13}$	$< 7.3 \times 10^{13}$
W2054+0207	$< 2.9 \times 10^{13}$	$< 9.2 \times 10^{13}$
W2357+0328	$< 1.9 \times 10^{13}$	$< 5.3 \times 10^{13}$

**Table 3.** Number of serendipitous sources in each of the 10 maps at greater than  $3\sigma$  and  $4\sigma$  significance, and the number of negative peaks at greater than  $3\sigma$  significance. There were no negative peaks at greater than  $4\sigma$  in the 10 maps.

Source	Number of Serendipitous Sources at greater than $3\sigma$	Number of Serendipitous Sources at greater than $4\sigma$	Number of Negative Peaks at greater than $3\sigma$
W0831+0140	3	0	0
W1136+4236	1	0	0
W1603+2745	1	0	0
W1814+3412	1	0	1
W1835+4355	1	0	0
W2026+0716	2	1	1
W2054+0207	3	0	1
W2216+0723	2	0	0
W2246-0526	1	0	1
W2357+0328	2	0	0